Combined experimental and modelling studies of proton conducting La1-xBa1+xGaO4-x/2: proton location and dopant site selectivity

Kendrick, Emma; Knight, K. S.; Islam, M. S.; Slater, Peter

DOI:
10.1039/C0JM02039G

Combined experimental and modelling studies of proton conducting $La_{1-x}Ba_{1+x}GaO_{4-x/2}$: proton location and dopant site selectivity.

E. Kendrick[1], K.S. Knight[2], M. S. Islam[3], P.R. Slater[4]*

[1]Chemical Sciences, University of Surrey, Guildford, Surrey, U. K. GU2 7XH

[2]ISIS Facility, Rutherford Appleton Laboratory, Harwell Science and Innovation Campus,

Didcot, OX11 0QX. UK

[3]Department of Chemistry, University of Bath, Bath, U.K. BA2 7AY

[4]School of Chemistry, University of Birmingham, Birmingham, U.K. B15 2TT

Correspondence to

Dr. P.R. Slater
School of Chemistry, University of Birmingham, Birmingham, U.K. B15 2TT

p.r.slater@bham.ac.uk

Abstract

In this paper, neutron diffraction studies are reported on the $La_{1-x}Ba_{1+x}GaO_{4-x/2}$ system in order to locate the proton sites. Difference Fourier maps suggested the presence of unfitted nuclear density (negative for H_2O treated samples, and positive for D_2O treated samples) adjacent to the O3 and O4 sites, giving sensible O-H/D distances. The results therefore indicate more than one proton site, consistent with modelling studies which suggested that there was little difference between the proton defect energies for different oxygen sites. The results indicate a mixture of inter- and intra-tetrahedra H bonding interactions, with the shortest interaction being of the order of 2 Å. Further modelling studies into dopant site selectivity are also reported which indicate that charge and size effects dominate the solution energies.

Key words: gallate, neutron diffraction, proton conduction

1. Introduction

Proton conducting oxides have been attracting considerable attention, due to their importance in a range of applications such as solid oxide fuel cells (SOFC's), hydrogen sensors and hydrogen separation membranes [1]. The research to date has concentrated mainly on materials which possess the perovskite type structure (AMO_3) in particular $BaMO_3$ (where M=Zr, Ce). In such systems, oxide ion vacancies are introduced by acceptor doping with trivalent cations at the M cation site. With the introduction of oxide ion vacancies, water incorporation can then occur leading to the introduction of protons (equation 1)

$$H_2O + V_o^{\bullet\bullet} + O_o \leftrightarrow 2OH_o^{\bullet} \quad (1)$$

Despite the high interest in these perovskite systems, they are not without their problems, in particular high grain boundary resistivities for M=Zr, and low stability for M=Ce [1]. Consequently there has been considerable interest in the development of new materials displaying high temperature proton conductivity. In this respect, materials containing tetrahedral moieities have attracted significant recent interest, including $LaMO_4$ (M=P, Nb, Ta] and $LaBaGaO_4$ [2-9]. In this paper, we report further detailed structural and modelling studies of the latter gallate system. This material has the β-K_2SO_4 structure [9], with discrete gallium tetrahedral units. Increasing the barium, lanthanum ratio in $LaBaGaO_4$ results in oxygen vacancies, and, as with the perovskite systems, protons are incorporated via water dissociation. Thus, significant proton conductivity ($\approx 10^{-4}$ Scm^{-1} at 500°C) has been reported in $La_{0.8}Ba_{1.2}GaO_{3.9}$ [7]. In prior work, we examined the accommodation of oxide ion vacancy defects in this system, showing that the introduction of such vacancies leads to the condensation of adjacent tetrahedra to give a Ga_2O_7 unit such that tetrahedral geometry around each Ga is maintained. Water incorporation can then occur leading to a break up of these units. DFT modelling work suggested that the protons were stabilised by inter-tetrahedra hydrogen bonding, leading to low activation energies for proton migration between tetrahedra, with

the rate determining process for long range proton migration being migration around the tetrahedra (intra-tetrahedra migration) [9]. In this work, we extend this modelling work to examine the energetics of dopant incorporation, in order to identify the most favourable dopants for future experimental work. We also present detailed neutron diffraction studies, with a view to locating the proton site in these systems. In order to improve the reliability of locating this site by neutron diffraction, two samples of $La_{0.8}Ba_{1.2}GaO_{3.9}$ were analysed, one slow cooled in O_2/H_2O and the other in O_2/D_2O. The high contrast between the scattering factors of H and D (hydrogen has a negative nuclear scattering length while deuterium has a positive nuclear scattering length) offers a useful confirmation for the proton site location [10, 11].

2. Experimental

A large sample of $La_{0.8}Ba_{1.2}GaO_{3.9}$ was synthesised using the solid state method, from intimately ground mixtures of La_2O_3 $BaCO_3$ and Ga_2O_3, which were heated to 950°C for 12 hours, reground and reheated twice at 1300°C for 12 hours. To obtain hydrated materials, this sample was split into two portions, one was heated to 500°C in O_2/H_2O, and one in O_2/D_2O. Neutron diffraction data were collected on the diffractometer, HRPD, ISIS, Rutherford Appleton Laboratory. Data sets from two banks of detectors were used for the refinement; the first was the data from the backscattering detector bank and the second was the data from the 90° detector bank. Both sets of banks were used in the refinement so as to increase the neutron counts and improve the potential identification of the proton site. The data were collected at a temperature of 4.2 K, in order to reduce the magnitudes of the thermal displacement parameters and hence allow the H/D site to be more readily located. All structural refinements were performed using the GSAS suite of programs [12].

In order to gain predictive information regarding suitable dopants, and dopant site selectivity, computer modelling calculations were performed. These computer simulation techniques of ionic conductors are well documented [13], and therefore only a summary of the computational techniques used in this work will be given. These computer simulations analysing dopant site

energies employed established atomistic techniques (as embodied in the GULP code [14]. The calculations are based on the Born model in which interactions between ions are evaluated in terms of long range Coulombic terms, and a short-range Buckingham potential (2), which takes account of Pauli repulsion and Van der Waals effects.

$$V_{ij}(r_{ij}) = A\exp(-r_{ij}/\rho) - C/r_{ij}^{6} \qquad (2)$$

In order to describe the ionic polarisability of the ions, the shell model was employed, in which a shell attached to the ionic core via a harmonic spring constant is used.

An important feature of these simulations is the treatment of lattice relaxation around the dopant ion, and in this respect the Mott– Littleton approach was employed, in which the crystal lattice is partitioned into two regions: the immediate environment surrounding the defect is relaxed explicitly, whilst the remainder of the crystal, where the defect forces are relatively weak, is treated by more approximate quasi-continuum methods. In this way the long range relaxation is effectively modelled and the crystal is not considered simply as a rigid lattice. Interatomic potentials were transferred directly from our previous study [9].

3 Results and discussion

3.1 Neutron diffraction structural studies: $La_{0.8}Ba_{1.2}GaO_{3.9}$ hydrated and deuterated.

The refined atomic positions for $LaBaGaO_4$ were used as the starting parameters, which resulted in a good initial fit to the data. In order to try to locate the H/D site, difference Fourier synthesis plots were performed in order to look for residual negative scattering (indicative of protium) and positive

scattering (indicative of deuterium) peaks. These plots gave three potential proton positions, one located adjacent to the O3 site and two located adjacent to the O4 site, leading to sensible (≈1 Å) O-H bond distances. These positions were therefore included in the refinement, with the thermal displacement parameters of the H atoms fixed at a sensible value, and the occupancies varied. The data suggested the presence of 0.12 H/D, leading to an increase in the oxygen content on hydration from 3.9 to 3.96. The presence of multiple proton sites is consistent with modelling studies, which suggested little energy differences between proton sites on different oxygens. The refined parameters and atomic positions are given in table 1, with selected bond lengths and angles are given in table 2, and the neutron diffraction profiles in figure 1. The data show the expected distorted GaO_4 environment, as well as indicating high atomic displacement parameters for the oxygen sites. The latter can be correlated with static disorder arising from the significant local distortions caused by the presence of the larger Ba^{2+} cation in place of La^{3+}, as well as the presence of protons, as highlighted by our previous modelling studies [9]. The structure, including the proton positions, is shown in figure 2. The successful location of the proton sites in such a complex structure with low proton content highlights the benefits of neutron diffraction using a combined H/D approach. The Ga-O-H bond angles range between 84 and 111°, indicating that the protons are pointing almost perpendicular to the Ga-O bond direction. The H-bonding interactions are between 2.0-2.3 Å, suggesting relatively weak H-bonding. Figure 3 highlights the H-bonding interactions illustrating a mixture of intra- and inter- tetrahedral H bonding. The shortest H-bonding interaction (2.0 Å) is the inter-tetrahedron interaction O3-H---O3, which is consistent with modelling work which highlighted the significance of inter-tetrahedra interactions [9]. The intra-tetrahedron interactions were all shown to be larger, at a distance of ≈2.3 Å.

3.2 Energetics of dopant incorporation in $La_{1\pm x}Ba_{1\pm x}GaO_{4\pm x/2}$

In order to identify future doping strategies to enhance the ionic conductivity of these materials, as well as to produce potential mixed proton/electronic conductors, with applications as electrode materials, hydrogen separation membranes, a range of cation dopants were analysed for each of the cation sites in the structure, and the solution energies determined. Where appropriate energies of oxide ion vacancy, interstitial defects were taken from our previous study [9].

3.2.1 M^{2+} dopant substitution

If substitution of a divalent dopant occurs on a lanthanum or gallium site, charge compensation occurs in the form of an oxygen vacancy whilst substitution for barium requires no charge compensation. The equations for the substitution reactions are therefore

$$MO + La_{La} \rightarrow M'_{La} + \tfrac{1}{2}V_O^{\bullet\bullet} + \tfrac{1}{2}La_2O_3 \quad (3)$$

$$MO + Ga_{Ga} \rightarrow M'_{Ga} + \tfrac{1}{2}V_O^{\bullet\bullet} + \tfrac{1}{2}Ga_2O_3 \quad (4)$$

$$MO + Ba_{Ba} \rightarrow M_{Ba} + BaO \quad (5)$$

Figure 3 shows a plot of the solution energy for substitution against the ionic radii of the dopant cation. The ionic radii is taken from Shannon [15] (data for 6 coordination is taken, as ionic radii for this coordination is quoted for all cations). The data shows that the most favourable substitution is on the Ba site, since this gives no oxide ion vacancies, with favourable energy particularly for the large dopants, e.g. Sr. For the dopants on the La site and Ga site, large cations (e.g. Ba) favour the former, while small cations the latter. This is consistent with experimental work where the successful incorporation of Ba to give $La_{1-x}Ba_{1+x}GaO_{4-x/2}$ is known. Further studies on partial Sr substitution for Ba are warranted from these predictions, although it should be noted that complete replacement of Ba by Sr leads to $LaSrGaO_4$ with the K_2NiF_4 (octahedral Ga) rather than β-K_2SO_4 structure (tetrahedral Ga).

3.2.2 M^{3+} dopant substitution

Substitution of a M^{3+} dopant for lanthanum or gallium requires no charge compensation, while substitution for barium requires charge compensation in the form of either the incorporation of oxygen interstitials or cation vacancies; in all cases the solution energy was lower for charge compensation by oxygen interstitials. The equations for the substitution reactions are given in equations (5-7).

$$\tfrac{1}{2}M_2O_3 + La_{La} \rightarrow M_{La} + \tfrac{1}{2}La_2O_3 \qquad (5)$$

$$\tfrac{1}{2}M_2O_3 + Ba_{Ba} \rightarrow M_{Ba} + BaO + \tfrac{1}{2}O_i^{''} \qquad (6)$$

$$\tfrac{1}{2}M_2O_3 + Ga_{Ga} \rightarrow M_{Ga} + \tfrac{1}{2}Ga_2O_3 \qquad (7)$$

The results, as illustrated in figure 4, showed that M^{3+} substitution for barium appears unfavourable. In contrast the energies for La^{3+} substitution suggested more favourable solution energies, particular for the larger lanthanide cations, Pr^{3+} and Nd^{3+}, which has been confirmed by experiment [8]. For the Ga site, low substitution energies for aluminium and transition metal M^{3+} dopants were predicted, with the favourability increasing with decreasing ionic radii.

4. Conclusions

In this work, we have examined neutron diffraction data for deuterated and hydrated samples of $La_{0.8}Ba_{1.2}GaO_{3.9}$ to locate the proton site(s), with 3 positions shown, consistent with previous modelling studies which suggested a range of stable proton sites. Further modelling work into dopant incorporation suggests that, as expected, charge and size effects dominate the solution energies.

Acknowledgements

We would also like to express thanks to EPSRC for funding and ISIS for the provision neutron diffraction beam time.

References

1. 1. K.D. Kreuer,, *Annual Review of Materials Research*; 33 (2003) 333.
2. N. Kitamura, K. Amezawa, Y. Tomii, N. Yamamoto; *Solid State Ionics* **2003**, *162-163*, 161
3. H.R. Haugsrud, T. Norby, *Nat. Mater.* **2006**, *56*, 193.
4. T. Mokkelbost, I. Kaus, R. Hausgrud, T. Norby, T. Grande, M.A. Einarsrud; *J. Amer. Ceram. Soc.* **2008**, *91*, 879.
5. A. Kuwabara, R. Haugsrud, S. Stolen, T. Norby.; *Phys. Chem. Chem. Phys*. 11 (2009) 5550.
6. N. Kitamura, K. Amezawa, Y. Tomii. *J. Electrochem. Soc.* 152 (2005) A658
7. S.Li, F. Schönberger, P.R. Slater; *Chem. Commun*. 21 (2003) 2694.
8. F. Schönberger, E. Kendrick, M.S. Islam, P.R. Slater, *Solid State Ionics* 176 (2005) 2951.
9. E. Kendrick, J. Kendrick, K. S. Knight, M. S. Islam, P. R. Slater ; *Nature Mater*. 6 (2007) 871.
10. K.S. Knight, *Solid State Ionics*, 127 (2000) 43.
11. E. Kendrick, K.S. Knight, M.S. Islam, P.R. Slater; Solid State Ionics 178 (2007) 943.
12. A.C. Larson, R.B. Von Dreele. *Los Alamos National Laboratory, Report*. No LA-UR-86-748 (1987).
13. *Computer Modelling in Inorganic Crystallography*. Ed. C. R. A. Catlow, Academic press, San Diego, CA, 1997.
14. J.D. Gale, A.L. Rohl, The General Utility Lattice Program, *Mol. Simul.*, **29**, 291-341 (2003).
15. R.D. Shannon, *Acta Crystallographica*. A 32 (1976) 751.

Table 1. Final refined structural parameters for $La_{0.8}Ba_{1.2}GaO_{3.9}/H_2O$ from neutron powder diffraction studies.

Atom	x	y	z	Ui/Ue*100 ($Å^2$)	Site occ.
Ba1	0.6721(2)	0.3345(2)	0.245(1)	1.70(4)	1.0
Ba2/La2	0.0488(1)	0.4952(2)	0.2492(6)	1.41(4)	0.2/0.8
Ga1	0.3342(1)	0.2795(2)	0.2605(6)	1.61(3)	1.0
O1	0.1766(2)	0.1549(2)	0.254(1)	*	1.0
O2	0.4270(3)	0.2174(9)	0.4866(7)	*	1.0
O3	0.2889(3)	0.5020(5)	0.3749(5)	*	0.96
O4	0.4395(3)	0.2139(8)	0.0020(7)	*	1.0
H1	0.5040	0.1529	0.1256	2.5	0.026(6)
H2	0.3858	0.2189	0.8709	2.5	0.030(5)
H3	0.2551	0.5129	0.0399	2.5	0.066(5)

* Anisotropic thermal parameters ($Å^2$)

Atom	100 x U11	100 x U22	100 x U33	100 x U12	100 x U13	100 x U23
O1	0.37(8)	2.7(1)	6.8(1)	-0.98(9)	0.7(3)	1.4(3)
O2	2.0(2)	9.9(4)	1.0(2)	-1.6(2)	-0.2(2)	2.4(2)
O3	2.2(2)	3.3(2)	8.2(2)	1.2(2)	-0.7(1)	-1.6(2)
O4	1.5(2)	8.0(4)	2.0(2)	2.4(2)	0.1(2)	1.1(2)

R_{wp}	5.31%
R_p	4.76%
^{2}	2.22
Space Group	$P2_12_12_1$
a	10.06848(7) Å
b	7.36694(6) Å
c	5.95098(5) Å

Table 2. Selected bond lengths and angles for $La_{0.8}Ba_{1.2}GaO_{3.9}/H_2O$ from neutron powder diffraction studies.

Bond	**Distance/Å**
Ba1_O1	2.974(9)
Ba1_O1	2.983(9)
Ba1_O1	2.810(2)
Ba1_O2	2.985(5)
Ba1_O2	3.049(5)
Ba1_O2	3.295(6)
Ba1_O3	2.583(4)
Ba1_O4	2.896(5)
Ba1_O4	3.092(5)
Ba1_O4	3.367(6)
Ba2/La2_O1	2.818(2)
Ba2/La2_O1	2.556(2)
Ba2/La2_O2	2.536(5)
Ba2/La2_O2	2.643(6)
Ba2/La2_O3	2.531(3)
Ba2/La2_O3	2.763(4)
Ba2/La2_O4	2.412(5)
Ba2/La2_O4	2.621(5)
Ga1_O1	1.835(2)
Ga1_O2	1.701(5)
Ga1_O3	1.833(4)
Ga1_O4	1.931(5)
O4-H1	1.079(4)
O4-H2	0.951(4)
O3-H3	1.083(3)
Bond Angle	**Angle (°)**
O1_Ga1_O2	111.0(2)
O1_Ga1_O3	103.8(1)
O1_Ga1_O4	109.5(2)
O2_Ga1_O3	94.8(3)
O2_Ga1_O4	105.1(1)
O3_Ga1_O4	131.1(2)

Figure legends

Figure 1. Observed, calculated, and difference profiles for $La_{0.8}Ba_{1.2}GaO_{3.9}/H_2O$

Figure 2. The Structure of $La_{0.8}Ba_{1.2}GaO_{3.96}H_{0.12}$, showing the location of the proton positions (Tetrahedra = GaO_4, Pink spheres = La, Red spheres = Ba, White spheres = O, Black spheres = H).

Figure 3. Illustration of H-bonding interactions, showing a mixture of inter-tetrahedra and intra-tetrahedra interactions.

Figure 4. Solution energies for M^{2+} dopants from atomistic simulations.

Figure 5. Solution energies for M^{3+} dopants from atomistic simulations.

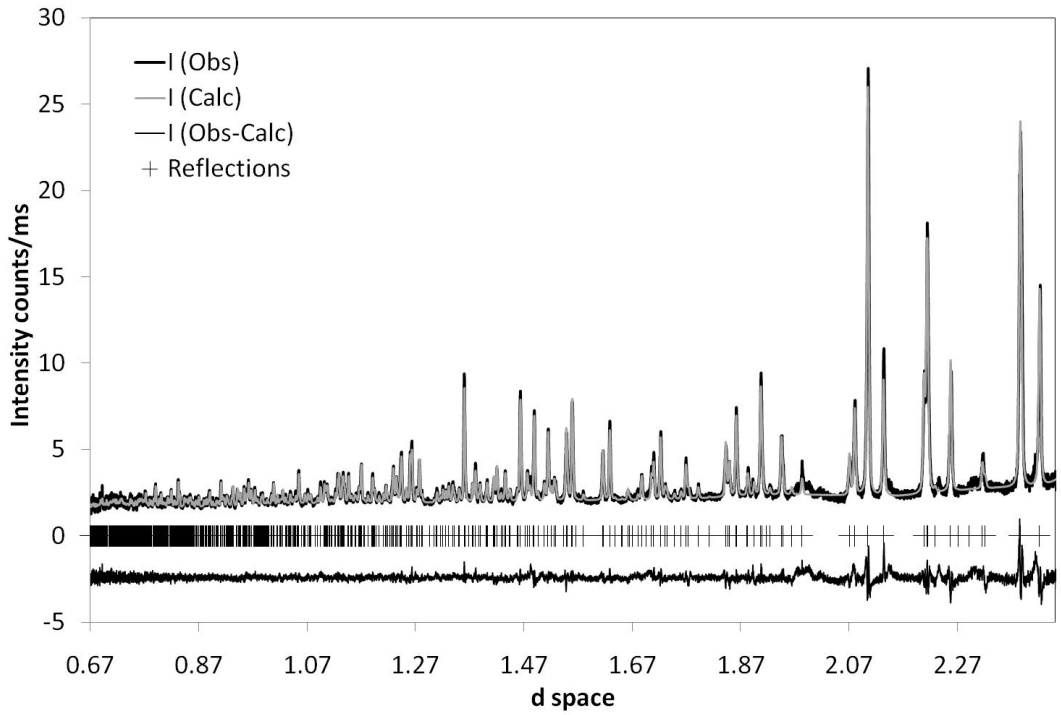
I (Obs)
I (Calc)
I (Obs-Calc)
Reflections
Intensity counts/ms
30
25
20
15
10
5
0
-5
0.67
0.87
1.07
1.27
1.47
1.67
1.87
2.07
2.27
d space

Fig 1

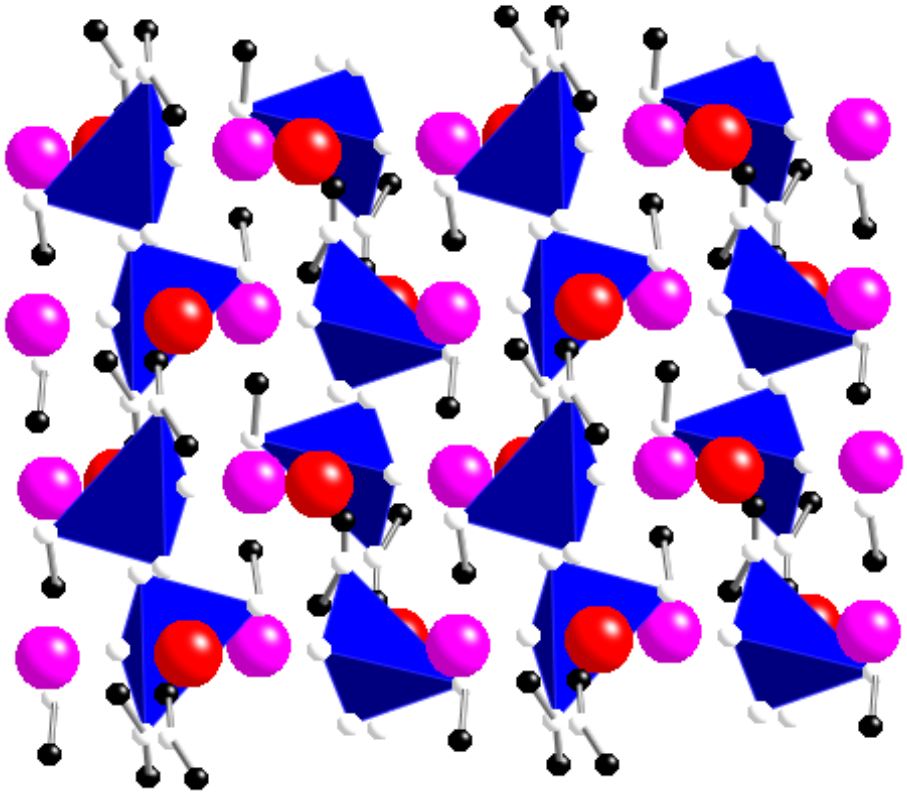

Fig. 2

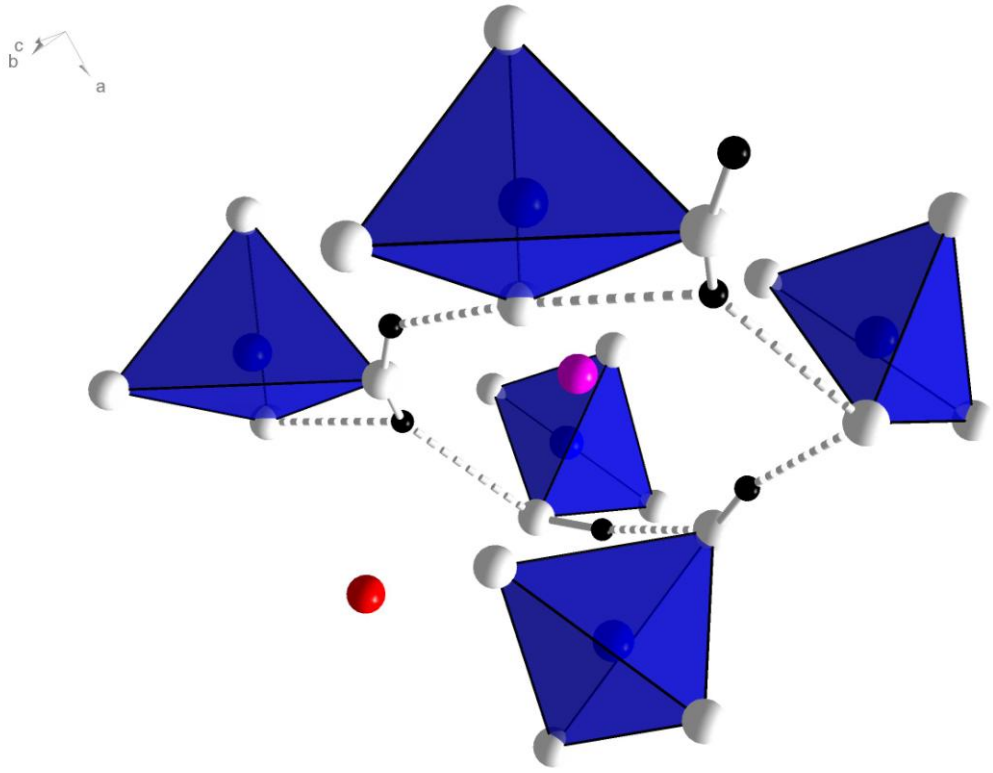

Fig. 3

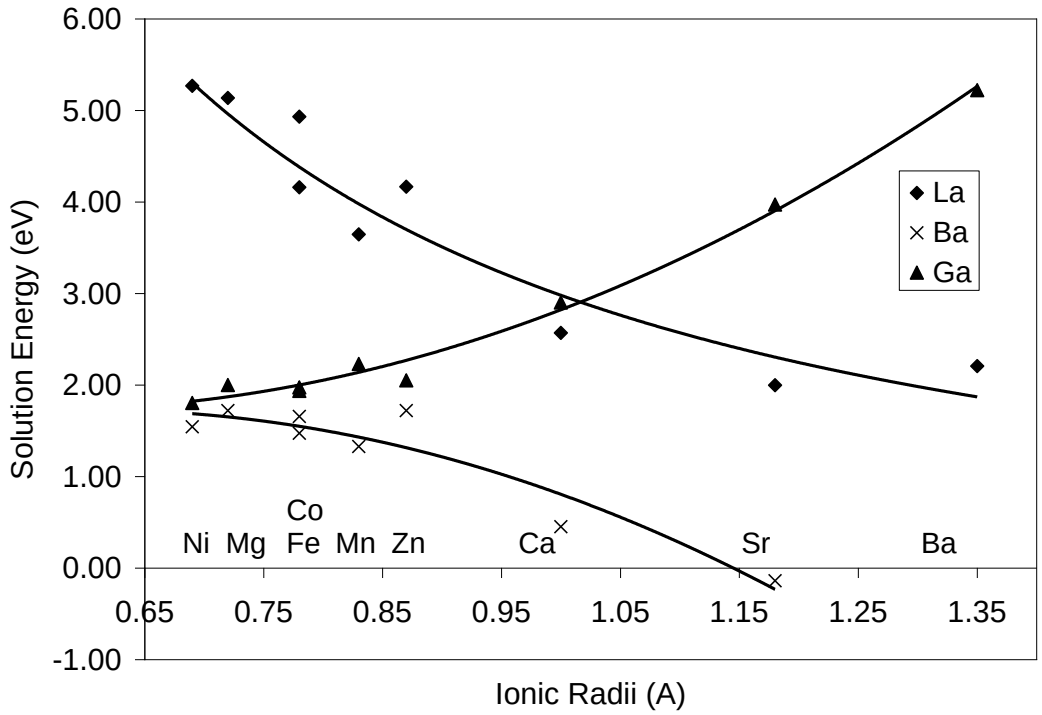
6.00
5.00
4.00
3.00
2.00
1.00
0.00
-1.00
Solution Energy (eV)
0.65
0.75
0.85
0.95
1.05
1.15
1.25
1.35
Ionic Radii (A)
Ni
Mg
Co
Fe
Mn
Zn
Ca
Sr
Ba
La
Ba
Ga

Fig. 4

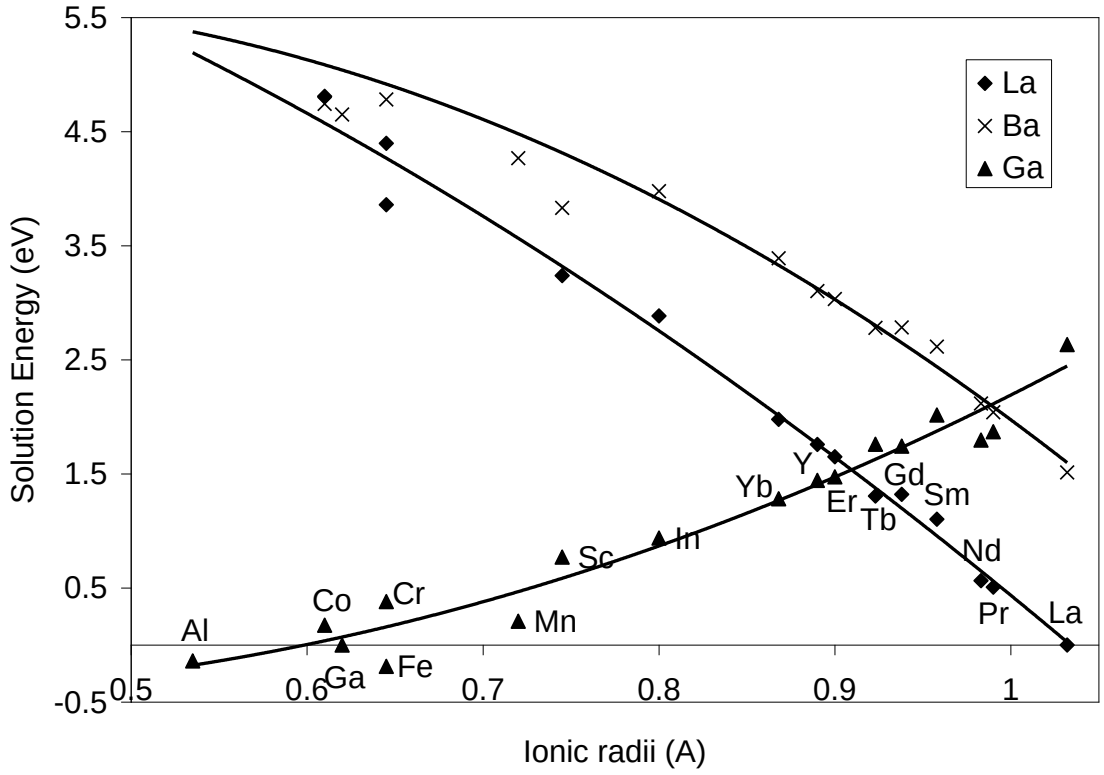
5.5
4.5
3.5
2.5
1.5
0.5
-0.5
Solution Energy (eV)
0.5
0.6
0.7
0.8
0.9
1
Ionic radii (A)
La
Ba
Ga
Y
Yb
Gd
Sm
Er
Tb
Nd
Pr
La
In
Sc
Co
Cr
Mn
Al
Ga
Fe

Figure 5.